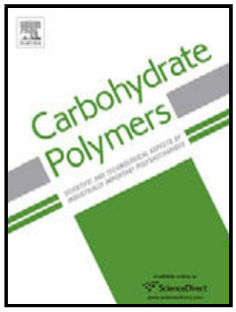

Title: Self-assembly of nitrogen-doped carbon dots anchored on bacterial cellulose and their application in iron ion detection

Authors: Pengfei Lv, Yixin Yao, Dawei Li, Huimin Zhou, Muhammad Awais Naeem, Quan Feng, Jieyu Huang, Yibing Cai, Qufu Wei

PII: S0144-8617(17)30486-1
DOI: http://dx.doi.org/doi:10.1016/j.carbpol.2017.04.086
Reference: CARP 12274

To appear in:

Received date: 10-2-2017
Revised date: 8-4-2017
Accepted date: 25-4-2017

Please cite this article as: Lv, Pengfei., Yao, Yixin., Li, Dawei., Zhou, Huimin., Naeem, Muhammad Awais., Feng, Quan., Huang, Jieyu., Cai, Yibing., & Wei, Qufu., Self-assembly of nitrogen-doped carbon dots anchored on bacterial cellulose and their application in iron ion detection.*Carbohydrate Polymers* http://dx.doi.org/10.1016/j.carbpol.2017.04.086

Self-assembly of nitrogen-doped carbon dots anchored on bacterial cellulose and their application in iron ion detection

Pengfei Lv[a], Yixin Yao[a], Dawei Li[a], Huimin Zhou[a], Muhammad Awais. Naeem[a], Quan Feng[b], Jieyu Huang[a], Yibing Cai[a], Qufu Wei[a]*

E-mail addresses: 18861800875@163.com (P. Lv); 18801510310@163.com (Y. Yao); ldw19900323@163.com (D. Li); xjzhouhuimin@126.com (H. Zhou); mawaisnaeem@hotmail.com (M.A. Naeem); fengquan@ahpu.edu.cn (Q. Feng); 18861823219@163.com (J. Huang); yibingcai@163.com (Y. Cai); qfwei@jiangnan.edu.cn (Q. Wei)

[a] Key Laboratory of Eco-textiles, Jiangnan University, Wuxi 214122, China

[b] Key Laboratory of Textile Fabric, Anhui Polytechnic University, Wuhu, Anhui 241000, China

Highlights

- As-prepared N-CDs shows excellent optic properties.
- As-prepared BC/N-CDs were applied to the detection of Fe^{3+} in aqueous solution via sustainable one-step method of biosynthesis..
- This fluorescence sensor shows high sensitive response in acceptable range of 0.5-600 μM and ultralow detection limit of 84 nM.
- This work expands application scopes of both bacterial cellulose and fluorescence materials.

Abstract: Nitrogen-doped carbon dots (N-CDs) were synthesized through a facile hydrothermal method using citric acid (CA) and ethanediamine (EDA) as precursors. A green and simple fluorescence biosensor was obtained by biosynthesis of bacterial cellulose (BC)/N-CDs. As-prepared N-CDs with rich functional groups exhibited a blue emission under the excitation wavelength of 350 nm. Biosynthesis of BC/N-CDs were analyzed by Digital photos, Fourier Transform Infrared (FTIR) and Transmission Electron Microscopy (TEM). The results indicated that N-CDs were

successfully anchored on BC. As-prepared BC/N-CDs were applied to the detection of Fe^{3+} in aqueous solution. Spectroscopic data revealed that, fluorescence materials prepared presented an sensitive response to Fe^{3+} in acceptable range of 0.5-600 μM and ultralow detection limit of 84 nM as a fluorescence sensor. Furthermore, the results also indicate that a novel BC/N-CDs composite has great potential for the detection of Fe^{3+} ions based on membrane fluorescence materials.

Keywords: Bacterial Cellulose; Carbon dots; Fluorescence; Sensor; Detection

1. Introduction

It is well known that heavy metal ions cause serious harm to human health. Exploiting accurate, rapid and highly-efficient heavy metal ions detection methods have hence attracted global attention. Previous studies have looked at spectrophotometry, atomic adsorption spectrometry and inductively coupled plasma mass spectrometry for metal detection. Nevertheless, these traditional methods have their drawbacks, such as complicated analysis procedure, poor selectivity, fixed cumbersome instruments, and so forth. Fluorescent probes containing fluorescent nanoparticles, as an advanced analytical instrumental methodology, have been widely used for applications related to catalyses, energy, medicine and electronics (Shi et al. 2015). These can interact with various metals, leading to a change in the fluorescence intensity, and thus exploited to design a fluorescent sensor. However, these fluorescent probes usually consist of poisonous and expensive metal semiconductor materials. Thus, finding low-cost and eco-friendly alternate materials is key to long term success.

Carbon quantum dots (CDs) possess similar fluorescent properties to other semiconductor quantum dots and simultaneously possess excellent benefits such as biocompatibility, water solubility, chemical stability, and low toxicity. Based on these advantages, CDs have been widely applied in medical diagnosis, bio-imaging, catalysis, photovoltaic devices, and sensor technologies (Kong et al. 2012). When

CDs are combined with specific metals, these two materials form a sort of complex and the fluorescence intensity of the CDs will decrease, referred to as "turn-off" phenomenon, which can be ascribing to the quenching behavior of CDs. Based on this aspect of CDs, a variety of fluorescent sensors for detection of metals, including Fe^{3+}, a ubiquitous metal in nature, using CDs have been reported. Miao and coauthors reported a facile electrochemical synthesis method of CDs from ethanol, which was further applied for the detection of Fe^{3+} (Miao et al. 2015). Yang and coauthors reported an innovative and green strategy to synthesize CDs with 19.8% of quantum yield originated from honey, and the obtained CDs were used to detect Fe^{3+} with a low detection limit of 1.7×10^{-9} mol/L and a linear range of 5.0×10^{-9}-1.0×10^{-4} mol/L (Yang et al. 2014). A simple and efficient hydrothermal carbonization of *Prunus avium* fruit extract for the synthesis of the fluorescent nitrogen-doped carbon dots (N-CDs) for detection of Fe^{3+} was described by Edison and coauthors (Edison et al. 2016).

Nevertheless, CDs usually aggregate in solution thus compromising their properties. Moreover, the solution environment is not beneficial to separation and post-treatment of CDs. Thus, combining CDs with solid substrate materials to preserve sensing property of CDs is a research hot topic. Up to now, there have been a few reports on the combination of CDs with membrane substrates. Shi and co-authors used filter paper as the substrate material for the immobilization of CDs, and obtained CD-anchored fluorescent filter paper (Shi et al. 2015). However, the relatively poor adhesion force between CDs and filter paper severely restricts repeated use of the novel substrate. Li et al. reported a carbon quantum dot encapsulated mesoporous silica/polyacrylonitrile electrospun nanofibrous membrane, successfully employed for the analysis of Fe^{3+} in aqueous environment (Li et al. 2016). Junka et al. reported the proof-of-concept for the synthesis of a transparent and fluorescent nanopaper displaying a tunable luminescence as confirmed by confocal microscopy imaging (Junka et al. 2014). Bian et al. reported cellulose-based fluorescent materials using zinc sulfide quantum dot-decorated graphene by a one-step hydrothermal method (Bian et al. 2016). Although the CDs were encapsulated inside the fibers, the opaque

outer wall of nanofiber reduced the overall fluorescent properties. Meanwhile, compared to CDs, chemical doping of the CDs surface with heteroatoms is an effective approach to manipulate optical and chemical properties because of the strong electron-withdrawing behavior exerted by, for example, nitrogen-doping (Yan et al. 2011).

Bacterial cellulose (BC), synthesized by bacteria, is a low-cost and eco-friendly biomacromolecules (Klemm et al. 2001; Lv et al. 2016; Shah et al. 2013; Soykeabkaew et al. 2009). Compared with conventional fibers, BC has many unique advantages, such as large specific surface area, high crystallinity, good biocompatibility, and high mechanical strength (Ge et al. 2015; Lin et al. 2013; Pircher et al. 2014). In addition, wet BC lacks nearly any opacity, which is beneficial for any fluorescent-based design.

In this work, N-CDs were synthesized via the hydrothermal method using citric acid (CA) and ethanediamine (EDA) as precursors firstly. After that, a novel BC/N-CDs composite membrane was developed by a economical and convenient one-pot synthesis method. The morphologies, structures and properties of obtained N-CDs and BC/N-CDs composite membrane were characterized. Besides, the BC/N-CDs composite membrane was successfully applied in the detection of Fe^{3+} in water environment by analyzing the change of fluorescence intensity of BC/N-CDs composite membrane. In sum, this work provides a simple, effective and eco-friendly method for the construction of luminescent N-CDs on BC membranes with high detectability for detection Fe^{3+}. Meanwhile, the satisfactory fluorescence analysis results suggest that the BC/N-CDs composite membrane may provide a candidate for fluorescent probe of heavy metal ions based on solid membrane materials.

2. Experimental

2.1. Materials

Yeast extract, Bacto peptone were obtained from Sigma Aldrich (USA). D-mannitol sodium, NaCl, $NiCl_2$, $ZnCl_2$, $AgNO_3$, $CdCl_2$, $MnSO_4$, $FeCl_3$, $Co(NO_3)_2$, $MgSO_4$, KCl, $PbCl_2$, $FeCl_2$, $CaCl_2$ and $CuCl_2$ were purchased from Sinopharm

Chemical Reagnent. Co., Ltd. (China). All of the chemicals were of analytical grade and solutions were prepared with distilled water.

2.2. Instrumentation

Field emission scanning electron microscopy (FE-SEM) images were performed using a Hitachi S-4800 (Tokyo, Japan) at 1.0 kV. Elemental and chemical structure of all samples were analyzed by Fourier transform infrared spectroscopy (FTIR, Nicolet Nexus, Thermo Electron Corporation, Waltham, MA, USA) with KBr as a sample, X-ray diffraction (XRD, Bruker AXS D8, Germany) and X-ray photoelectron spectroscopy (XPS, Escalab 250Xi, Thermo Scientific Escalab, USA) with monochromatized Al ka radiation. The BC/N-CDs composite membrane was dispersed into deionized water using ultrasonic cell disruptor (JY 98-111DN, China). Dispersed samples were dropped onto copper grids and examined by a high-resolution transmission electron microscope (HR-TEM, JEOL/JEM-2100, Tokyo, Japan). The UV/Vis spectra were performed with a U-3000 spectrophotometer (Hitachi, Japan). Fluorescence imaging of all samples were recorded on a Hitachi F-7000 spectrometer (Tokyo, Japan).

2.3. Preparation of fluorescent N-CDs

The N-CDs were prepared from the precursors of CA and EDA by hydrothermal treatment. The typically procedure of synthesis of fluorescent N-CDs was as follows (P et al. 2017; Zhu et al. 2013), 3.6 g CA and 0.2 mL EDA were dissolved into 120 mL deionized water in 200 mL beaker by stirring for 30 min to uniformly dispersed. Then mixture was added into a Teflon-lined autoclave for 5 h at 220 °C using hydrothermal treatment. Subsequently, the reaction flask was cooled to room temperature. The precipitate was centrifuged at 4000 rpm for 5 min, then repeated three times to obtain the pale yellow supernatant and the product with the light yellow suspension was further purified in a dialysis bag for 24 h to obtain N-CDs liquid. Finally, the obtained N-CDs were further concentrated up to 10 mg/mL in deionized water.

2.4. Self-assembly of N-CDs anchored on BC

Firstly, N-CDs were added into culture media containing 0.3 wt% bacto-peptone,

0.5 wt% yeast extract and 2.5 wt% D-mannitol. The culture solutions were sterilized at 120 °C in an autoclave for 2 h. The pre-cultured cells in a test tube containing *Gluconacetobacter xylinus* (***ATCC 10245***) were inoculated into a 100 mL Erlenmeyer flask with final concentrations 1 mg/100 mL N-CDs in culture solution. The flasks were incubated on a cultivation cabinet at 30 ˚C for 6 days. The synthesized BC/N-CDs were separated from the medium by filtration and were dipped into 1 wt% NaOH for 2 h at 100 °C in order to remove the microorganism and culture medium embedded in the cellulose material, and then repeatedly rinsed to neutral in pure water. Finally, the BC/N-CDs usually are stored in deionized water or ethylalcohol and used by freezing-drying by freezing dryer.

3. Results and discussion

3.1. Cultivation process analysis

As illustrated in Fig. 1(A,B), After adding *G. xylinus* and N-CDs into a 100 mL Erlenmeyer flask which contained 10 mL of HS medium with 1 mg/100 mL N-CDs, the growth of cultures (both static and agitated) formed was observed for six consecutive days. The pictures were taken in a dark room by using a 350 nm ultraviolet lamp as an excitation source (Fig. 1(A, B)). On day one, the culture solution was a completely transparent blue-colored liquid (Fig. 1(A)) that became more nepheloid over time. On the 6th day, the surface of culture solution began to present membrane under fluorescent lamp, indicating the gradual formation of BC/N-CDs composite membrane. Fig. 1(B) shows the formation process of "spheroid" in the presence of N-CDs under agitated conditions. Compared to Fig. 1(A), the culture solution displays same colored (on the first day), ascribing to little or no growth of BC. As time passed by (Day 2), the culture solution shows turbid, attributing to the generation and reproduction of some single BC fibrils and *bacteria*. From 3rd to 5th day, the culture solution was semi-lucent while concomitantly "spheroid" formation at the bottom of culture solution occurred, attributing to growth of self-assembly BC/N-CDs. On 6th day, the bottom of culture solution began to display plentiful "spheroids", as shown in Fig. 1(B). It also can be clearly seen that

the remaining N-CDs were incorporated into BC membrane (Fig. 2 (B,C)), indicating that the BC/N-CDs membrane could be used in luminescent patterning and related applications. Fig. 1(C) shows the cultivation of BC pellicle with N-CDs. The first day, *G. xylinus* and N-CDs were added into the culture solution and obtained a stable dispersion under static conditions. To start with, the *bacteria* were attached on the surface of air bubbles, after that, they began to reproduce *bacteria* while concomitantly little or no BC growth (Czaja et al. 2004). With increase of *bacteria* multiplication and BC growth, N-CDs were attached to single BC fibrils surface created a monolayer BC/N-CDs composites structure, which may be attributed to hydrogen-bond interaction with materials itself, as shown in Fig. 1(C). Subsequently, the monolayer BC/N-CDs composites were surrounded by gathered *bacteria* while concomitantly the reproduction of *bacterial* and increase of BC fibrils. This self-assembly of N-CDs on BC and formation of BC/N-CDs composites successively interlinked and progressively accumulated to obtained a far more tight multilayered structure. With increase of time, the BC/N-CDs-formation rate became slow, ascribed to reduced oxygen. The formation of new BC/N-CDs composites membrane on existing pellicle was continuous until more overlapped, compact and uniform fibrils were formed (Nandgaonkar et al. 2014). The whole culture process led to a homogeneous membrane or an irregular “spheroid” shaped composite with a multilayer overlapped structure under static, agitated conditions, as illustrated in Fig. 2.

3.2. Morphological analysis

Fig. 3(A) displays the digital photos of pure BC under incandescent lamp. BC membrane was transparent while BC had three dimensional interconnected nanofibrous networks and an average size of about 40 nm, as shown in the size distribution (inset) of Fig. 3(C). Fig. 3(C) clearly shows BC membrane retains porous networks structure with numerous intertwined ultrathin nanofibrous, while concomitantly endowing large surface area and rich hydroxyl (-OH) groups for N-CDs anchored on BC by the strong hydrogen bonding (Wang et al. 2012), as illustrated in Fig. 3(B). Fig. 3(B) reveals digital photos of BC in the presence of

N-CDs under UV light (350 nm). BC membrane was found to be translucent while BC/N-CDs composite membrane exhibit a blue luminescence and quite homogeneous, which clearly indicates a good dispersion of N-CDs inside the BC nanofibrous network surely due to the second order interactions, such as electrostatic interactions and hydrogen bonding. It can be clearly seen from TEM image that the N-CDs display spherical shape and the average size of the microspheres is 1.83 nm, as shown in Fig. 3(F). Fig. 3(E) shows some N-CDs were anchored on BC fibrous surfaces, while some others aggregated to form large size of N-CDs, which may have been caused by the inter-attraction of the N-CDs during the self-assembly process.

3.3. Chemical structures analysis

Fig. 4(A) shows the XRD diffraction patterns of pure BC and N-CDs in BC samples for comparison. The broad diffraction peaks at 14.5° and 22.6°, as shown in Fig. 4(A), were corresponded to crystallographic planes marked as (100), and (110) reflection of BC (Castro et al. 2015), respectively. Compared with pure BC, the XRD of BC/N-CDs had no significant change as it slightly moved towards higher locations and broadened. The broad diffraction peaks at 22.6° for BC/N-CDs sample heighten and broaden, attributing to amorphous carbon ordered in a considerably random fashion the disorder carbon of N-CDs (Wei et al. 2013), as illustrated in Fig. 4(A). Fig. 4(B) shows the FITR spectra of BC and BC/N-CDs composites. The characteristic peaks at 3337 cm^{-1} indicated the O-H group, ascribing to stretching vibration in O-H (Li et al. 2014a). The peak around 2893 cm^{-1} was assigned to C-H stretching (Gadim et al. 2014). The peaks at 1028, 1053, 1108 and 1160 cm^{-1} were typically those of cellulose, ascribing to the C6-O6, C3-O3, C2-O2 and C1-O-C4 glycosidic link, respectively. Compared to BC, a group of characteristic bands of N-CDs could be indexed in the BC/N-CDs composites, suggesting a successful self-assembly. The following absorption peaks can be seen: stretching vibrations of C-N at 1423 cm^{-1}, bending vibrations of N-H at 1645 cm^{-1}, and stretching vibrations of C=O at 1724 cm^{-1} (Li et al. 2014b). Compared with BC, the characteristic peaks around 3400 cm^{-1} were enhanced, attributing to stretching vibrations of O-H and N-H (Wang et al. 2014), as can be seen in Fig. 4(B). Those characteristic absorption peaks reveal that there are

numerous hydroxyl groups (-OH), carbonyl group (C=O) and amino-containing ($-NH_2$) functional groups on N-CDs surface, resulting in the good hydrophilic properties of N-CDs while concomitantly hydrogen bonding actions of BC and N-CDs by self-assembly.

XPS was used to analyze the elements and structure of BC/N-CDs films, as illustrated in Fig. 4(C). Fig. 4(C) indicates three crucial peaks at 532, 400, and 285 eV, corresponding to the binding energies of O1s, N1s, and C1s (Hu et al. 2016), respectively. This indicates that the BC/N-CDs are mainly composed of O, N and C. The contents of the three elements of BC/N-CDs were displayed as follows: 38.72% (O), 3.24% (N) and 58.04% (C), respectively. Meanwhile, the high-resolution spectrum of C1s further confirm that the presence of four peaks at 284.3, 285.4, 286.5 and 287.8eV, which were assigned to C-C(sp^3), C-N and C-O/C=O bonds, respectively (Gu et al. 2015), as illustrated in Fig. 5(A). The N(1s) element of the high-resolution spectrum are illustrated in Fig. 5(B). Fig. 5(B) displays the three major peaks occurred at 399.5, 400.5 and 401eV, attributing to C-N-C, N-C3 and N-H bonds, respectively (Gong et al. 2014). The high-resolution spectrum of O(1s) was de-convoluted into two binding peaks at 531.3 and 532.4eV, ascribing to C=O and C-OH/C-O-C groups, respectively, as shown in Fig. 5(C). FTIR and XPS results indicated that N-CDs were functionalized by nitrous groups ($-NH_2$), hydroxyl (-OH) and (-C=O) groups.

3.4. Spectral properties of N-CDs

Fig. S1(A) displays two absorption bands locating at 350 nm and 240 nm, ascribing to the n-π* transition of C=O and π-π* transition of carbon core, respectively (Dan et al. 2015). A strong absorption band at 350 nm is consistent with the maximum excitation wavelength at 350 nm. Hence, the N-CDs presented a bright blue color under UV light at 350 nm, as shown in the inset photograph of Fig. S1 (D). Excitation-dependent PL behavior is common for fluorescent materials . To further study co-relation between excitation wavelength and emission wavelength, the fluorescent spectra of N-CDs were recorded as the excitation wavelength over 280-480 nm. The fluorescent emission spectra of N-CDs varied systematically from

350 nm to 600 nm, which presented change in the PL intensity, as shown in Fig. S1(B). It clearly reveals that N-CDs achieved the maximum emission intensity around 440 nm when it was excited at 350 nm. The complexity of the PL behavior is attributed to the surface size, resulting in further effect on the band gap of N-CDs. Hence, excitation-dependent PL behavior can be useful in biosensors applications.

The effect of fluorescence intensity of N-CDs with the variation of pH was evaluated, and surprisingly important optical responses to changes in pH were recorded using a spectrofluorimeter. A series of fluorescent N-CDs samples with pH ranging systematically from 3.5 to 7.5 were prepared, while concomitantly the fluorescence intensity of fluorescent N-CDs at different values of pH was recorded. Dramatically changes in emission intensity were revealed as the pH varied, as illustrated in Fig. S1(C). Fig. S1(C) obviously shows that the fluorescent intensity of N-CDs prominently enhanced with the pH increases from 3.5 to 7, reaching to an optimum value around pH=7. However, the fluorescent intensity slightly decreased as the variation of pH from 7 to 7.5, which is corresponded to the uniformly dissolution of N-CDs at low pH values while concomitantly the aggregation of CDs with the increase of pH, attributing to non-covalent molecular interactions of N-CDs. In summary, the emission peak position slightly shifted to left for the excitation wavelength (280-480 nm) and different pH (3.5-7.5), ascribing to the electronic effect of the surface groups. Meanwhile, the PL was found strongly dependent as excitation wavelength and pH varied. The relation of the fluorescent intensity of N-CDs with different N-CDs concentration ranging from 0 μg/mL to 250 μg/mL was also recorded, as illustrated in Fig. S1(D). The increased N-CDs concentration resulted in the increase of fluorescent intensity of N-CDs, ascribed to the number of increase of quantum dots.

To analyze the sensing properties of N-CDs to metal ions, the PL intensities of N-CDs under the excitation at 350 nm in the presence of representative metal ions were subsequently measured after incubation for 10 min, including Na^{+}, Ni^{2+}, Zn^{2+}, Ag^{+}, Cd^{2+}, Mn^{2+}, Fe^{3+}, Co^{2+}, Mg^{2+}, K^{+}, Pb^{2+}, Fe^{2+}, Ca^{2+} and Cu^{2+} (1 mM), as illustrated in Fig. 6. The as-prepared N-CDs displayed high selectivity to Fe^{3+}. Fig.

6(A) remarkably reveals completely quenched phenomenon in presence of Fe^{3+} into N-CDs dispersion, which may be ascribed to the quickly chelating effect of functional groups of N-CDs surface with Fe^{3+} ions (Zhao et al. 2014). In contrast, the addition of other metal ions has no obvious quenching effect which can be detected by the naked eye, and all of those presented blue color. The above results indicated that as-prepared N-CDs-based fluorescence materials possessed high selectivity towards Fe^{3+} and can be better applied in sensor toward metal detection. As shown in Fig. 6(B), the variation of fluorescence intensity of N-CDs after adding different metal ions were further recorded by a spectrofluorimeter. The fluorescence intensity of N-CDs in presence of Fe^{3+} ion was close to constant (0). Meanwhile, the fluorescence changes ratio $(I_0\text{-}I)/I$ is immediately revealed in Fig. 6(C), which I_0 and I are defined as the fluorescence intensities of as-prepared N-CDs at 350 nm in the absence and presence of metal ions, respectively.

3.5. Sensing properties of BC/N-CDs

3.5.1. Selectivity study

To further investigate the optical properties of BC/N-CDs composites, the fluorescent intensity of BC/N-CDs was measured, as shown in Fig. 7(A). Compared to the fluorescence intensity of BC membranes, self-assembly of N-CDs anchored on BC membranes showed relatively improved value, suggesting that incorporation or absorption of N-CDs into or upon the BC membranes was successful. The effect of time on fluorescent intensity of BC/N-CDs was also further studied and the results are displayed in Fig. 7(B). The fluorescent intensity of BC/N-CDs nanocomposites exhibited remarkable stability, with almost no change observed with the passage of time, as illustrated in Fig. 7(B). The initial fluorescent intensity was 1574 a.u. and the fluorescent intensity was about 1539 a.u. after 60 days. The residual fluorescent intensity of BC/N-CDs retained about 97.8% of their original value after 60 days. In general, self-assembled BC/N-CDs are considered to be comparatively stable fluorescent membrane materials. To further investigate the sensing properties of BC/N-CDs to metal ions, the fluorescent intensity of BC/N-CDs membrane was recorded, as shown in Fig. 7(C). Fig. 7(C) shows there was significant PL quenching

with the addition of Fe^{3+} into BC/N-CDs membrane materials. Compared with other metal ions, the PL quenching phenomenon of BC/N-CDs membrane is consistent with the synthesis of N-CDs, with no significant quenching effect, as illustrated in Fig. 7(C). The effect of pH on the performance of the BC/N-CDs-Fe^{3+} was studied, As shown in Fig. 7(D), F and F_0 were defined as the fluorescent intensity of BC/N-CDs in the presence of pH ranging systematically from 3.5 to 9 and the fluorescent intensity of BC/N-CDs membrane materials (pH=7), respectively. It clearly revealed that the fluorescence quenching of the BC/N-CDs-Fe^{3+} was effective for pH ranging from 3.5 to 9. Under low pH conditions, the organic moieties of N-CDs surface might be protonated and resulted in the high positively charged surface (Bhattacharya et al. 2015). Therefore, it will be difficult to achieve attachment of positively charged Fe^{3+} with N-CDs. Hence, the fluorescence quenching of BC/N-CDs was inefficient at low pH conditions. With increase of pH, the fluorescence quenching efficiency of BC/N-CDs membrane improved attributing to the deprotonation process by which functional surface of N-CDs is slowly taken over. Consequently, the negative charged carboxyl groups can attract the Fe^{3+} with opposite charge. Up to the limit of pH, it is very interesting that the fluorescence quenching of BC/N-CDs is inefficient, ascribing to the formation of deposit ($Fe(OH)_3$).

3.5.2. Analysis of Fe^{3+}

The sensitivity of BC/N-CDs membrane materials toward the Fe^{3+} ions analysis were recorded by fluorescence titrations after 10 min of incubation. The fluorescence intensity spectra of the BC/N-CDs with different concentrations of Fe^{3+}, as illustrated in Fig. 8(A). The fluorescence intensity of the BC/N-CDs membrane was gradually quenched as the concentrations of Fe^{3+} ions increased (0-900μM). Fig. 8(B) shows a good linear relationship between the fluorescence intensity ratio (F_0/F) and the concentrations of Fe^{3+} from 0 to 600μM. The corresponding regression coefficient (R^2) between different concentrations of Fe^{3+} ions and the fluorescence intensity is 0.997 (n=4). This result reveals that BC/N-CDs possess high selectivity to Fe^{3+}. Meanwhile, the quenching efficiency of the Fe^{3+} ions was calculated as following the regression equation (1):

$$F_0 / F = 1.0514 + 0.011 * C_{Fe}^{3+} \quad (1)$$

Where F and F_0 are the fluorescence intensity of BC/N-CDs in the presence and absence of Fe^{3+}, respectively). The detection limit (LOD) of the BC/N-CDs membrane materials towards Fe^{3+} ion was calculated by employing following equation (2):

$$LOD = \frac{3\sigma}{K} \quad (2)$$

Where σ is the standard deviation of (F_0/F) values and *k* represents the slope of the linear line. The LOD of Fe^{3+} was estimated to be 84 nM at a signal-to-noise ratio of 3. Overall, the results revealed a relatively higher sensitive membrane sensors.

Based on BC/N-CDs membrane materials, there exists interaction between the molecule of cellulose (-OH) and the functional groups of N-CDs surfaces (-OH, -COOH and $-NH_2$) by hydrogen bonding, resulting in N-CDs anchored on bacterial cellulose membranes, as shown in Fig. 8(C). Moreover, as reported in previous literature studies, the possible fluorescence quenching mechanism of BC/N-CDs was studied with Fe^{3+}, as illustrated in Fig. 8. The functional groups ($-NH_2$, -COOH, -OH) of N-CDs surface might easily chelate with Fe^{3+} (Qu et al. 2013), formed a stable Fe^{3+}-complexes. Further, the formation of a stable chelate complex might change electron-hole or energy transfer from the surface of N-CDs, leading to BC/N-CDs composites fluorescence quenching:

Compared with different carbon-based fluorescent materials to detect Fe^{3+} as previously reported in various studies, the linear ranges and detection limits of BC/N-CDs is displayed, as shown in Table S1. The BC/N-CDs fluorescent materials endowed themselves satisfactory detection properties to Fe^{3+}. In summary, the novelty membrane fluorescent materials may be a promising candidate for practical applications of metal ions detection.

4. Conclusion

In summary, a typical method has been successfully explored to synthesize N-CDs using CA and EDA by hydrothermal treatment. As-prepared N-CDs were incorporated

for the first time into BC membrane via sustainable one-step method of biosynthesis. The results from various analyses indicated that N-CDs displayed superior optical properties while concomitantly exhibited excellent biocompatibility. The obtained BC/N-CDs composite membrane presented a good sensitive response towards Fe^{3+} ensuring the need of future research on the use of membrane for multifarious applications including luminescent indicator, recyclable test paper, green sensors and so on. Furthermore, we hope above results would be helpful to lead towards novel applications of membrane fluorescence materials.

Acknowledgements

This research was financially supported by the National Natural Science Foundation of China (51641303), the 111 Project (B17021), the Priority Academic Program Development of Jiangsu Higher Education Institutions, the Natural Science Foundation of Jiangsu Province (BK20150155), and the Fundamental Research Funds for the Central Universities (JUSRP51621A) and the Department of Education in Anhui Province of China (2015LJRCTD001).

Supplementary data

Reference

Bhattacharya, A., Chatterjee, S., Khorwal, V., Mukherjee, T.K. (2015). Luminescence turn-on/off sensing of biological iron by carbon dots in transferrin. Physical Chemistry Chemical Physics, 18(7), 5148-5158.

Bian, Y., He, B., Li, J. (2016). Preparation of cellulose-based fluorescent materials using Zinc sulphide quantum dot-decorated graphene by a one-step hydrothermal method. Cellulose, 23(4), 2363-2373.

Castro, C., Cordeiro, N., Faria, M., Zuluaga, R., Putaux, J.L., Filpponen, I., Velez, L., Rojas, O.J., Gañán, P. (2015). In-situ glyoxalization during biosynthesis of bacterial cellulose. Carbohydrate Polymers, 126(1), 32-39.

Czaja, W., Romanovicz, D., Brown, R.M. (2004). Structural investigations of microbial cellulose produced in stationary and agitated culture. Cellulose, 11(3), 403-411.

Dan, Q., Min, Z., Zhang, L., Zhao, H., Xie, Z., Jing, X., Haddad, R.E., Fan, H., Sun, Z. (2015). CORRIGENDUM: Formation mechanism and optimization of highly luminescent N-doped graphene quantum dots. Scientific Reports, 5(24), 7998-7998.

Edison, T.N.J.I., Atchudan, R., Shim, J.J., Kalimuthu, S., Ahn, B.C., Yong, R.L. (2016). Turn-off fluorescence sensor for the detection of ferric ion in water using green synthesized N-doped carbon dots and its bio-imaging. Journal of Photochemistry and Photobiology B-Biology, 158, 235-242.

Gadim, T.D., Figueiredo, A.G., Rosero-Navarro, N.C., Vilela, C., Gamelas, J.A., Barros-Timmons, A., Neto, C.P., Silvestre, A.J., Freire, C.S., Figueiredo, F.M (2014) Nanostructured bacterial cellulose-poly(4-styrene sulfonic acid) composite membranes with high storage modulus and protonic conductivity. Acs Applied Materials & Interfaces, 6(10), 7864-7875.

Ge, Y., Chen, S., Yang, J., Wang, B., Wang, H. (2015). Color-tunable luminescent CdTe quantum dot membranes based on bacterial cellulose (BC) and application in ion detection. Rsc Advances, 5(69), 55756-55761.

Gong, X., Lu, W., Man, C.P., Qin, H., Xin, W., Shuang, S., Dong, C., Choi, M.M.F. (2014). Facile synthesis of nitrogen-doped carbon dots for Fe^{3+} sensing and cellular imaging. Analytica Chimica Acta, 861, 74-84.

Gu, J., Hu, D., Wang, W., Zhang, Q., Zhen, M., Jia, X., Kai, X. (2015). Carbon dot cluster as an efficient “off–on” fluorescent probe to detect Au(III) and glutathione. Biosensors & Bioelectronics, 68, 27-33.

Hu, X., An, X., Li, L. (2016). Easy synthesis of highly fluorescent carbon dots from albumin and their photoluminescent mechanism and biological imaging applications. Materials Science & Engineering C-Materials for Biological Applications, 58, 730-736.

Junka, K., Guo, J., Filpponen, I., Laine, J., Rojas, O.J. (2014). Modification of cellulose nanofibrils with luminescent carbon dots. Biomacromolecules, 15(3), 876-881.

Klemm, D., Schumann, D., Udhardt, U., Marsch, S. (2001). Bacterial synthesized cellulose - artificial blood vessels for microsurgery. Progress in Polymer Science,

26(9), 1561-1603.

Kong, B., Zhu, A., Ding, C., Zhao, X., Bo, L., Yang, T. (2012). Carbon Dot‐Based Inorganic–Organic Nanosystem for Two‐Photon Imaging and Biosensing of pH Variation in Living Cells and Tissues. Advanced Materials, 24(43), 5844-5848.

Li, S., Huang, D., Yang, J., Zhang, B., Zhang, X., Yang, G., Wang, M., Shen, Y. (2014a). Freestanding bacterial cellulose–polypyrrole nanofibres paper electrodes for advanced energy storage devices. Nano Energy, 9, 309-317.

Li, S., Zhou, S., Xu, H., Xiao, L., Wang, Y., Shen, H., Wang, H., Yuan, Q. (2016). Luminescent properties and sensing performance of a carbon quantum dot encapsulated mesoporous silica/polyacrylonitrile electrospun nanofibrous membrane. Journal of Materials Science, 51(14), 6801-6811.

Li, Y., Zhong, X., Rider, A.E., Furman, S.A., Ostrikov, K. (2014b). Fast, energy-efficient synthesis of luminescent carbon quantum dots. Green Chemistry, 16(5), 2566-2570.

Lin, W.C., Lien, C.C., Yeh, H.J., Yu, C.M., Hsu, S.H. (2013). Bacterial cellulose and bacterial cellulose-chitosan membranes for wound dressing applications. Carbohydrate Polymers, 94(1), 603-611.

Lv, P., Wei, A., Wang, Y., Li, D., Zhang, J., Lucia, L.A., Wei, Q. (2016). Copper nanoparticles-sputtered bacterial cellulose nanocomposites displaying enhanced electromagnetic shielding, thermal, conduction, and mechanical properties. Cellulose, 23(5), 1-11.

Miao, P., Tang, Y., Han, K., Wang, B. (2015). Facile synthesis of carbon nanodots from ethanol and their application in ferric(III) ion assay. Journal of Materials Chemistry A, 3(29), 15068-15073.

Nandgaonkar, A.G., Wang, Q., Fu, K., Krause, W.E., Wei, Q., Gorga, R., Lucia, L.A. (2014). A one-pot biosynthesis of reduced graphene oxide (RGO)/bacterial cellulose (BC) nanocomposites. Green Chemistry, 16(16), 3195-3201.

P, L., Y, Y., H, Z., J, Z., Z, P., K, A., Y, C., Q, W. (2017). Synthesis of novel nitrogen-doped carbon dots for highly selective detection of iron ion. Nanotechnology, 28(16), 165502.

Pircher, N., Veigel, S., Aigner, N., Nedelec, J.M., Rosenau, T., Liebner, F. (2014). Reinforcement of bacterial cellulose aerogels with biocompatible polymers. Carbohydrate Polymers, 111(1), 505-513.

Qu, K., Wang, J., Ren, P.J., Qu, P.X. (2013). Carbon Dots Prepared by Hydrothermal Treatment of Dopamine as an Effective Fluorescent Sensing Platform for the Label-Free Detection of Iron(III) Ions and Dopamine. Chemistry, 19(22), 7243-7249.

Shah, N., Ulislam, M., Khattak, W.A., Park, J.K. (2013). Overview of bacterial cellulose composites: a multipurpose advanced material. Carbohydrate Polymers, 98(2), 1585-1598.

Shi, L., Li, Y., Li, X., Wen, X., Zhang, G., Yang, J., Dong, C., Shuang, S. (2015). Facile and eco-friendly synthesis of green fluorescent carbon nanodots for applications in bioimaging, patterning and staining. Nanoscale, 7(16), 7394-7401.

Soykeabkaew, N., Sian, C., Gea, S., Nishino, T., Peijs, T. (2009). All-cellulose nanocomposites by surface selective dissolution of bacterial cellulose. Cellulose, 16(3), 435-444.

Wang, C., Xu, Z., Cheng, H., Lin, H., Humphrey, M.G., Zhang, C. (2014). A hydrothermal route to water-stable luminescent carbon dots as nanosensors for pH and temperature. Carbon, 82, 87-95.

Wang, H., Zhu, E., Yang, J., Zhou, P., Sun, D., Tang, W. (2012). Bacterial Cellulose Nanofiber-Supported Polyaniline Nanocomposites with Flake-Shaped Morphology as Supercapacitor Electrodes. Journal of Physical Chemistry C, 116(24), 13013-13019.

Wei, J., Zhang, X., Sheng, Y., Shen, J., Huang, P., Guo, S., Pan, J., Liu, B., Feng, B. (2013). Simple one-step synthesis of water-soluble fluorescent carbon dots from waste paper. New Journal Chemistry, 38(3), 906-909.

Yan, L., Yang, Z., Huhu, C., Yue, H., Gaoquan, S., Liming, D., Liangti, Q. (2011). Nitrogen-Doped Graphene Quantum Dots with Oxygen-Rich Functional Groups. Journal of the American Chemical Society, 134(1), 15-18.

Yang, X., Zhuo, Y., Zhu, S., Luo, Y., Feng, Y., Dou, Y. (2014). Novel and green synthesis of high-fluorescent carbon dots originated from honey for sensing and imaging. Biosensors & Bioelectronics, 60(60), 292-298.

Zhao, A., Zhao, C., Meng, L., Ren, J., Qu, X. (2014). Ionic liquids as precursors for highly luminescent, surface-different nitrogen-doped carbon dots used for label-free detection of Cu^{2+} /Fe^{3+} and cell imaging ☆. Analytica Chimica Acta, 809, 128-133.

Zhu, S., Meng, Q., Wang, L., Zhang, J., Song, Y., Jin, H., Zhang, K., Sun, H., Wang, H., Yang, B. (2013). Highly photoluminescent carbon dots for multicolor patterning, sensors, and bioimaging. Angewandte Chemie-International Edition, 52(14), 3953-3957.

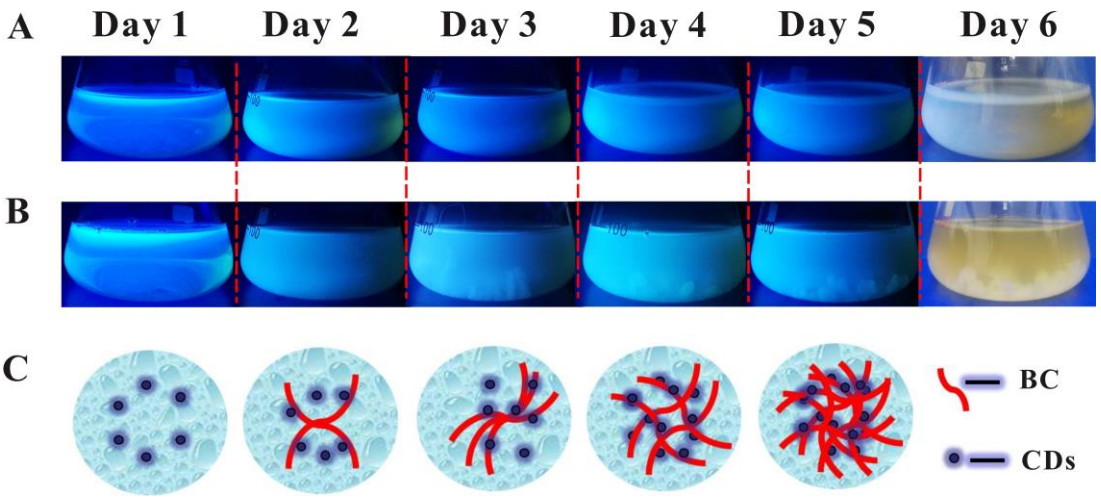

Fig. 1. The cultivation process of BC membrane containing N-CDs by *G. xylinus*: a photographic images of 5-days trace of BC growth: (A, B) static, agitated conditions by UV light (350 nm), respectively; the 6^{th} day growth of BC in the presence of N-CDs under fluorescent lamp; (C) A schematic illustration of BC/N-CDs formation.

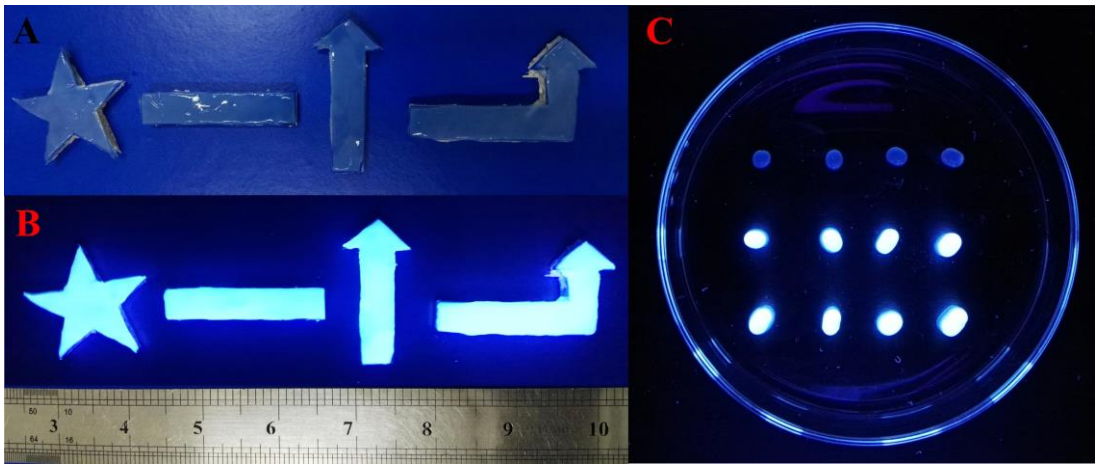

Fig. 2. Photographs of BC/N-CDs composites membranes. (A) Photos were taken under fluorescent lamp; photos were taken in a dark room by using a 350 nm ultraviolet lamp as an excitation source: (B) The “Indicator” pattern; (C) The “spheroid” pattern.

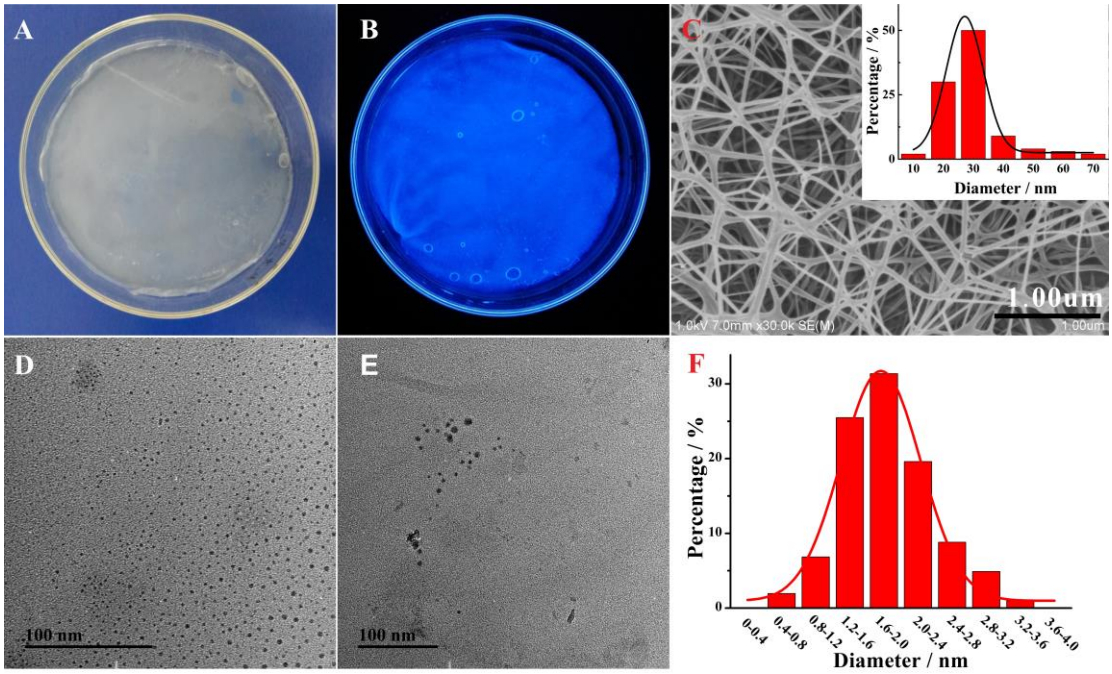

Fig. 3. Digital photos of BC in the presence of N-CDs: (A) Fluorescent lamp and (B) UV light (350 nm); (C) FESEM characterization of pure BC (inset: size distribution of BC); (D,E) TEM characterization of N-CDs and BC/N-CDs composite; (F) The size distribution of N-CDs.

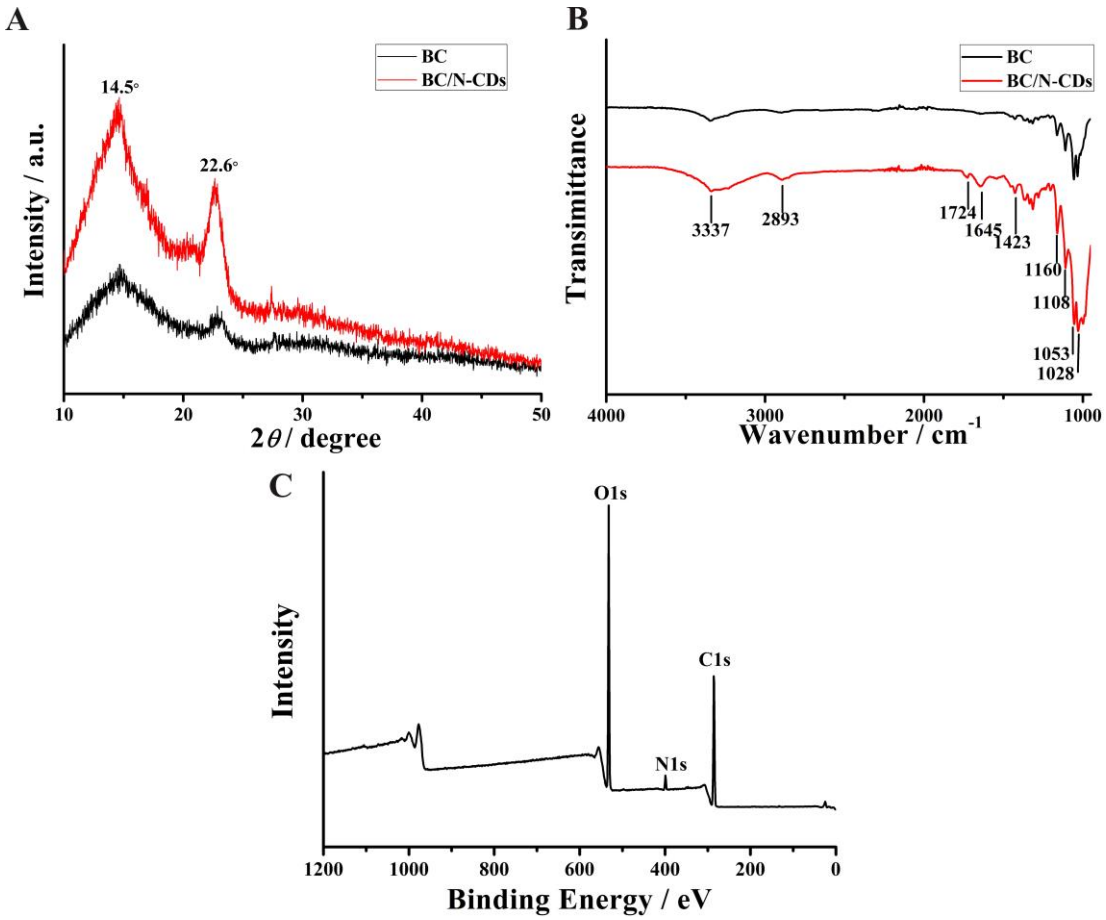

Fig. 4. (A) The XRD pattern; (B) FT-IR spectrum and (C) XPS spectrum of BC and BC/N-CDs sample.

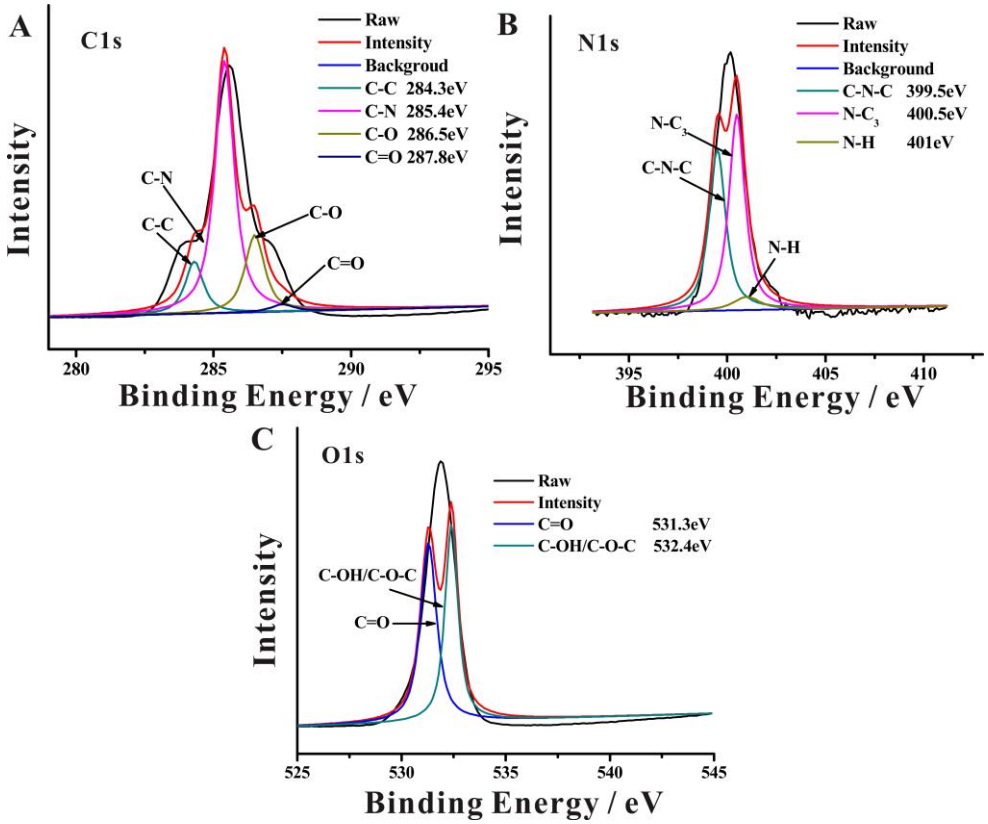

Fig. 5. High-resolution C1s (A), N1s (B) and O1s (C) peaks of BC/N-CDs.

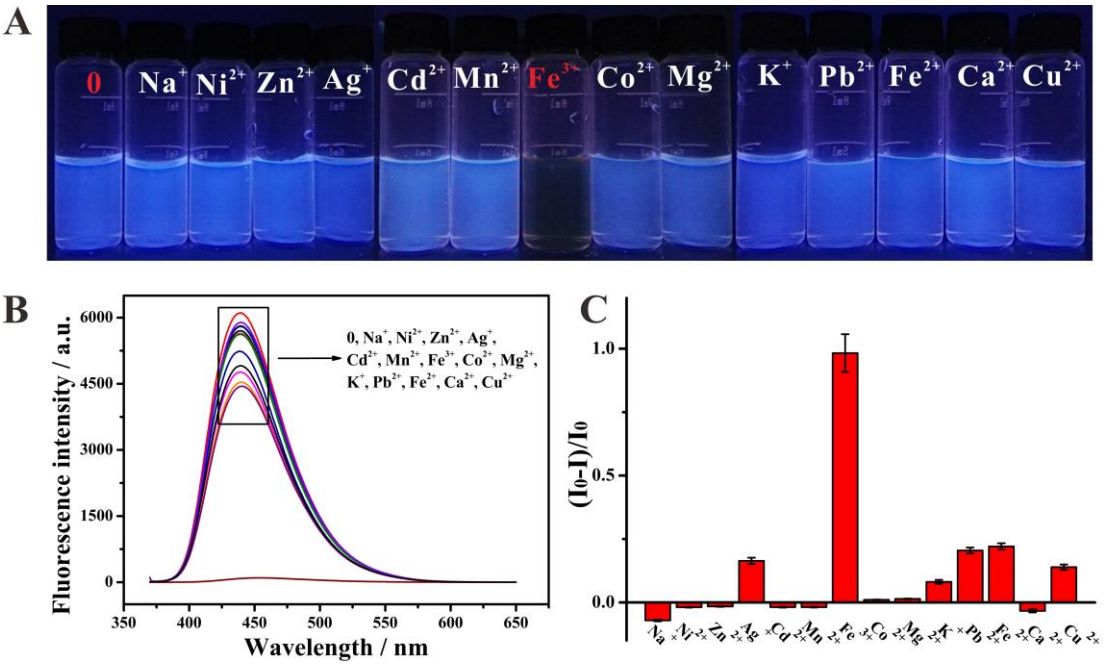

Fig. 6. (A) Fluorescence characterizations of CDs and CDs with different metal ions, (under the illumination of a 350 nm UV light); (B) Fluorescence spectra of CDs after adding 1 mM of metal salts in solutions; (C) The different $(I_0\text{-}I)/I_0$ values (fluorescence intensity ratio) of the CDs solution upon the condition that existing individual metal ions: Na^+, Ni^{2+}, Zn^{2+}, Ag^+, Cd^{2+}, Mn^{2+}, Fe^{3+}, Co^{2+}, Mg^{2+}, K^+, Pb^{2+}, Fe^{2+}, Ca^{2+}, Cu^{2+}.

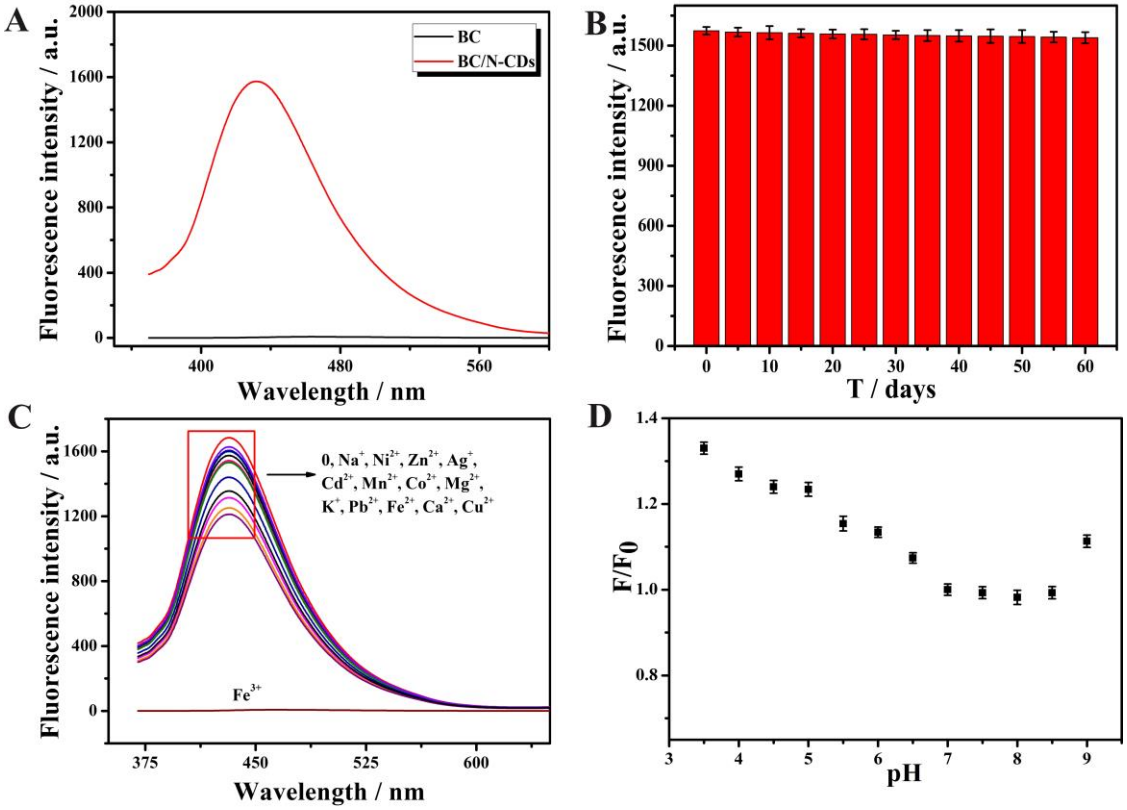

Fig. 7.（A）Fluorescence intensity change of BC membrane and BC/N-CDs under UV light of 350 nm; (B) The effect of time on the fluorenscence intensity of BC/N-CDs (0-60 days); (C) Fluorescence spectra of BC/N-CDs after adding 1 mM of metal salts in water solutions; (D)The effect of pH on the fluorenscence quenching of BC/N-CDs in the presence of Fe^{3+} to form BC/N-CDs-Fe^{3+} sensing system.

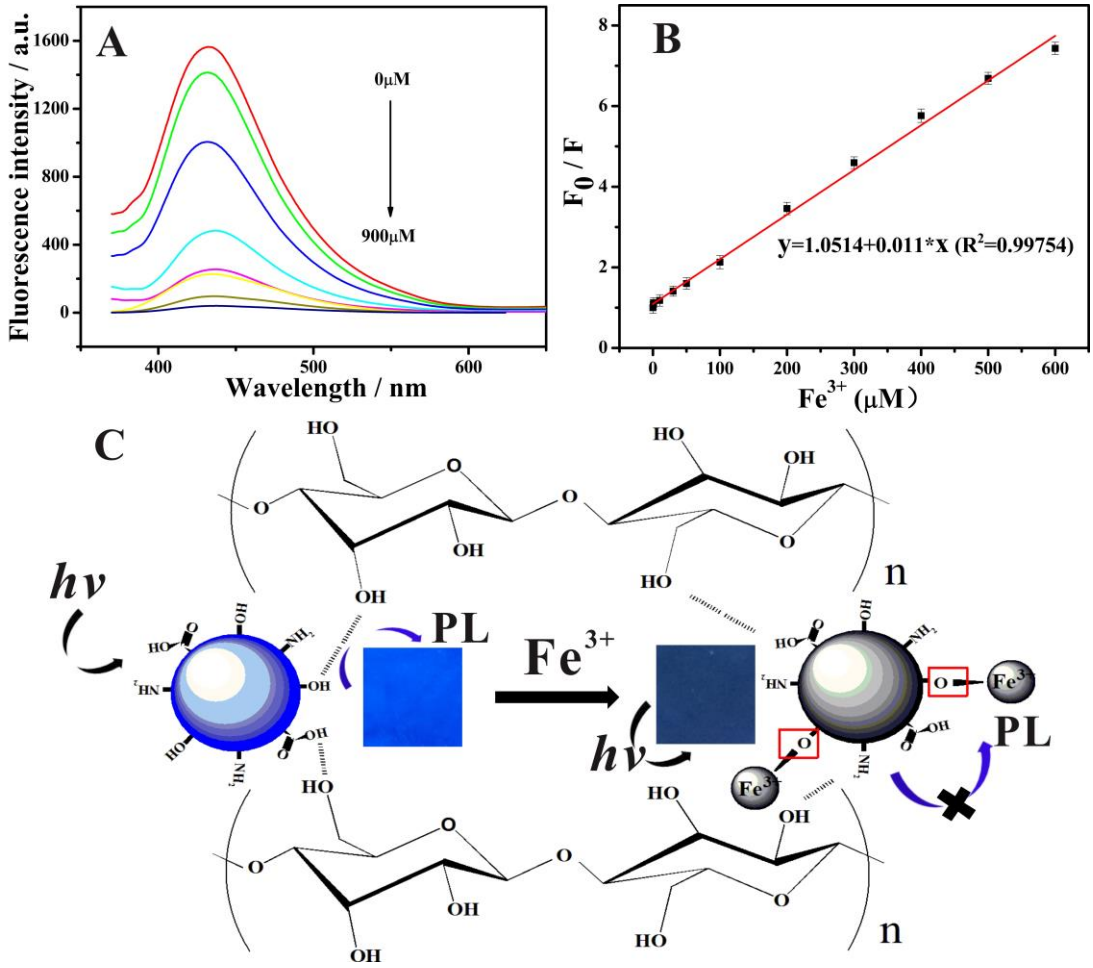

Fig. 8. (A) fluorescence spectra of BC/N-CDs in the presence of various concentrations Fe^{3+}(0-900μM); (B)The linear relationship between the F_0/F and Fe^{3+} concentration(0-600μM); (C) The schematic mechanism of the fluorescence quenching of BC/N-CDs to Fe^{3+} ions.